Dipole strength in ^{139}La below the neutron-separation energy

A. Makinaga,[1,*] R. Schwengner,[2] G. Rusev,[3] F. Dönau,[2] S. Frauendorf,[2,4] D. Bemmerer,[2] R. Beyer,[2] P. Crespo,[2,†] M. Erhard,[2,‡] A. R. Junghans,[2] J. Klug,[2,§] K. Kosev,[2] C. Nair,[2,‖] K. D. Schilling,[2] and A. Wagner[2]

[1]*Department of Physics, Konan University, Okamoto 8-9-1, Higashinada, Kobe 658-8501, Japan*

[2]*Institut für Strahlenphysik, Forschungszentrum Dresden-Rossendorf, D-01314 Dresden, Germany*

[3]*Department of Physics, Duke University, and Triangle Universities Nuclear Laboratory, Durham, North Carolina 27708, USA*

[4]*Department of Physics, University of Notre Dame, Notre Dame, Indiana 46556, USA*

(Received 4 June 2010; published 16 August 2010)

The γ-ray strength function is an important input quantity for the determination of the photoreaction rate and the neutron capture rate for astrophysics as well as for nuclear technologies. To test model predictions, the photoabsorption cross section of ^{139}La up to the neutron-separation energy was measured using bremsstrahlung produced at the electron accelerator ELBE of Forschungszentrum Dresden-Rossendorf with an electron beam of 11.5 MeV kinetic energy. The experimental data were analyzed by applying Monte Carlo simulations of γ-ray cascades to obtain the intensities of the ground-state transitions and their branching ratios. We found a significant enhancement of electric dipole strength in the energy range from 6 to 10 MeV that may be related with a pygmy dipole resonance. The present data are combined with photoneutron cross sections for ^{139}La and compared with results of calculations on the basis of a quasiparticle-random-phase approximation using an instantaneous-shape sampling.

DOI: 10.1103/PhysRevC.82.024314 PACS number(s): 25.20.Lj, 24.60.Dr, 26.50.+x, 27.60.+j

I. INTRODUCTION

The photodisintegration reaction plays an important role in astrophysics. In nature, there exist 35 neutron-deficient nuclides heavier than iron that cannot be produced via slow or rapid neutron capture and are referred to as p-process nuclei [1]. In the p process, the origin of heavy nuclei with $A < 100$ is considered to take place in white dwarf stars of binary systems or in the explosive proton-burning phase on the surface of neutron stars (rp process). In contrast, the production of nuclei with $A > 100$ is believed to take place in the O-Ne layers of massive stars. A possible reprocessing of the p-process matter may take place during their presupernova burning phases in type II supernovae or in the explosion of type Ia supernovae. The typical p-process temperature T is 1.7×10^9 K $< T < 3.3 \times 10^9$ K. At this temperature, the tail of the Planck distribution can induce photodisintegration reactions. In the photon bath, nuclei are thermally populated, whereas naturally, they exist in the ground state. In the statistical model, the calculation of the stellar reaction rate, which is the sum of the photodisintegration rates from all states weighted by the Boltzmann factor, requires the transmission coefficients of photons and any particles and the nuclear level densities (NLD). The transmission coefficient for electric dipole ($E1$) γ rays from excited nuclei is directly related to the $E1$ γ-ray strength function (GSF) [2]. In recent experiments, an enhancement of $E1$ strength around S_n has been found [3–10]. Such an enhanced strength causes the stellar reaction rate to increase significantly [11]. Therefore experimental cross sections for both the photon-scattering reaction below S_n and the photoneutron reaction above S_n become important quantities to determine the GSF.

The abundance of the rare odd-odd p-nucleus ^{138}La is generally underestimated in p-process calculations. Theoretical studies show that exploding sub-Chandrasekhar-mass CO white dwarfs and SNe-II are significant production sites for the nuclide ^{138}La [1,12]. The problem of the underproduction of ^{138}La is discussed in Refs. [1,13]. On the other hand, the ν process from ^{138}Ba via the weak charge-current reaction ^{138}Ba$(\nu, e)^{138}$La was proposed as the cosmic origin of ^{138}La, and an attempt was made to explain the underproduction of ^{138}La [1,13–15]. However, the photon-induced reaction rates remain a crucial parameter for the thermonuclear production of ^{138}La and ^{139}La.

The nuclide ^{139}La with a closed neutron shell at $N = 82$ is also of special importance for the understanding of nuclear structure. Dipole excitations at energies below 4 MeV were investigated in photon-scattering experiments at the former Stuttgart Dynamitron [16]. The dipole strength distribution at higher energy up to S_n is of particular interest because enhanced strength on the low-energy tail of the giant dipole resonance (GDR), often denoted as the "pygmy dipole resonance" (PDR), was found to be especially pronounced in neighboring $N = 82$ isotones [3,4] as well as in nuclides with $N = 50$ [6,8,9] and in ^{208}Pb with $N = 126$ [17,18].

Recently, photodisintegration cross sections for ^{139}La were measured by using quasi-monochromatic γ-ray beams from laser Compton back scattering at the National Institute of Advanced Industrial Science and Technology in Japan. Although the experimental data for ^{139}La$(\gamma,n)^{138}$La strongly constrained the stellar reaction rate on the ground-state target nucleus, the influence of the γ-ray strength close to the

*Present address: Hokkaido University, Sapporo 060-0810, Japan.

†Present address: LIP, Physics Department, University of Coimbra, P-3004-516 Coimbra, Portugal.

‡Present address: INFN, Sezione di Padova, I-35131 Padova, Italy.

§Present address: Vattenfall Power Consultant, S-16216 Stockholm, Sweden.

‖Present address: Nuclear Engineering Division, Argonne National Laboratory, Argonne, IL 60439.

 ©2010 The American Physical Society

neutron-separation energy on the stellar reaction rate remains an open question [19].

These circumstances motivated new measurements of photoabsorption cross sections of ^{139}La up to $S_n = 8.8$ MeV, which we present in the following. In Sec. II, we describe the experimental procedure and the data analysis. In Sec. III, the experimental results are compared with results of calculations on the basis of the quasiparticle random-phase approximation, including instantaneous-shape sampling [20], taking into account shape fluctuations in soft nuclei.

II. EXPERIMENTAL PROCEDURES

A. The photon-scattering experiment

The photon-scattering experiment on ^{139}La was performed using the bremsstrahlung facility [21] at the superconducting electron accelerator ELBE of the Forschungszentrum Dresden-Rossendorf (FZD). Bremsstrahlung was produced by hitting a 4 μm niobium radiator with an electron beam of 11.5 MeV kinetic energy and an average current of 520 μA. The bremsstrahlung beam was formed by an Al collimator with a conical drill hole of 8 mm diameter at the entrance and 24 mm at the outlet and a length of 2.6 m. A cylindrical Al absorber of 100 mm length was placed between the radiator and the collimator entrance to reduce the intensity of the low-energy part of the bremsstrahlung spectrum. The collimated photon beam impinged onto the target with a flux of several 10^8 MeV^{-1} s^{-1} in a spot of 38 mm diameter. The target was made of 3790 mg of natural La. It was sandwiched with 337.9 mg of ^{11}B enriched to 99.5% for the determination of the photon flux. Both materials were shaped to disks of 20 mm diameter to enable an irradiation with a constant flux density over the target area.

The scattered photons were measured with four high-purity germanium (HPGe) detectors of 100% efficiency relative to a NaI detector of 7.6 cm in length and 7.6 cm in diameter. All HPGe detectors were surrounded by escape-suppression shields made of bismuth germanate (BGO) scintillation detectors. To prevent γ rays scattered from surrounding materials from hitting the detectors, lead collimators of 10 cm thickness were placed in front of the detectors, and the BGO detectors were encased in cylindrically shaped lead layers of 2 cm thickness. Two HPGe detectors were placed vertically at 90° relative to the photon-beam direction at a distance of 28 cm from the target, resulting in opening angles of 16°. The other two HPGe detectors were placed horizontally at 127° to the beam at a distance of 32 cm from the target with opening angles of 14°. To reduce the intensities of scattered low-energy photons, absorbers of 13 mm Pb plus 3 mm Cu were placed in front of the detectors at 90° and 8 mm Pb plus 3 mm Cu were used for the detectors at 127°. Spectra of scattered photons were measured for 115 hours. Part of a spectrum, including events measured with the two detectors at 127° relative to the beam, are shown in Fig. 1.

B. Energy-integrated scattering cross sections

In photon-scattering experiments, the energy-integrated scattering cross section $I_s(E_x)$ of an excited state at the energy E_x can be deduced from the measured intensity of the respective transition to the ground state (elastic scattering). It can be determined relative to the known integrated scattering cross sections $I_s(E_x^{\mathrm{B}})$ of states in ^{11}B [22,23]:

$$\frac{I_s(E_x)}{I_s\left(E_x^{\mathrm{B}}\right)} = \left[\frac{I_\gamma(E_\gamma,\theta)}{W(E_\gamma,\theta)\Phi_\gamma(E_x)N_N}\right] \times \left[\frac{I_\gamma\left(E_\gamma^{\mathrm{B}},\theta\right)}{W\left(E_\gamma^{\mathrm{B}},\theta\right)\Phi_\gamma\left(E_x^{\mathrm{B}}\right)N_N^{\mathrm{B}}}\right]^{-1}. \quad (1)$$

Here $I_\gamma(E_\gamma,\theta)$ and $I_\gamma(E_\gamma^{\mathrm{B}},\theta)$ denote the measured intensities of a considered ground-state transition at E_γ and of a ground-state transition in ^{11}B at E_γ^{B}, respectively, observed at an angle θ to the beam. $W(E_\gamma,\theta)$ and $W(E_\gamma^{\mathrm{B}},\theta)$ describe the angular correlations of these transitions. The quantities N_N and N_N^{B} are the numbers of nuclei in the ^{139}La and ^{11}B targets, respectively. The quantities $\Phi_\gamma(E_x)$ and $\Phi_\gamma(E_x^{\mathrm{B}})$ represent the photon fluxes at the energy of the considered level and at the energy of a level in ^{11}B, respectively.

The integrated scattering cross section is related to the partial width of the ground-state transition Γ_0 according to

$$I_s = \int \sigma_{\gamma\gamma}\,dE = \left(\frac{\pi\hbar c}{E_x}\right)^2 g\frac{\Gamma_0^2}{\Gamma}, \quad g = \frac{2J_x+1}{2J_0+1}, \quad (2)$$

where $\sigma_{\gamma\gamma}$ is the elastic scattering cross section; E_x, J_x, and Γ denote energy, spin, and total width of the excited level, respectively; and J_0 is the spin of the ground state.

The determination of the level widths is hampered by three experimental difficulties. First, a considered level can be fed by transitions from higher lying states. The measured intensity of the ground-state transition is in this case higher than the one resulting from a direct excitation only. As a consequence, the integrated cross section deduced from this intensity contains a part originating from feeding in addition

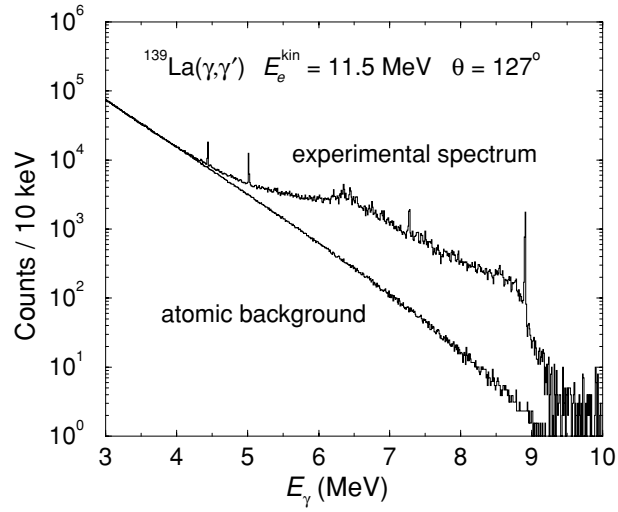

FIG. 1. Spectrum of photons scattered from ^{139}La, measured at 127° relative to the incident beam and corrected for room background and detector response, in comparison with the simulated spectrum of the atomic background multiplied with efficiency and measuring time. The prominent peaks at 4.443, 5.018, 7.280, and 8.912 MeV are transitions in ^{11}B.

to the true integrated scattering cross section: $I_{s+f} = I_s + I_f$. Second, a considered level can deexcite not only to the ground state but also to low-lying excited states (inelastic scattering). In this case, not all observed γ transitions are ground-state transitions. To deduce the partial width of a ground-state transition Γ_0 and the integrated absorption cross section, one has to know the branching ratio $b_0 = \Gamma_0/\Gamma$. If this branching ratio cannot be determined, only the quantity Γ_0^2/Γ can be deduced [cf. Eq. (2)]. Third, we cannot distinguish between dipole and quadrupole radiation, which have almost equal and nearly isotropic angular distributions when starting from the ground-state spin $J_0 = 7/2$. Hence the spins of the levels cannot be deduced, and the spin factor g [cf. Eq. (2)] cannot be calculated. Transitions observed in the present experiment and assigned to levels in ^{139}La are listed in Table I with the deduced integrated scattering cross sections and the quantities $g\Gamma_0^2/\Gamma$. Levels are given only for the energy range above about 5.5 MeV, where contributions from feeding to the integrated scattering cross sections become negligible [6,8,9].

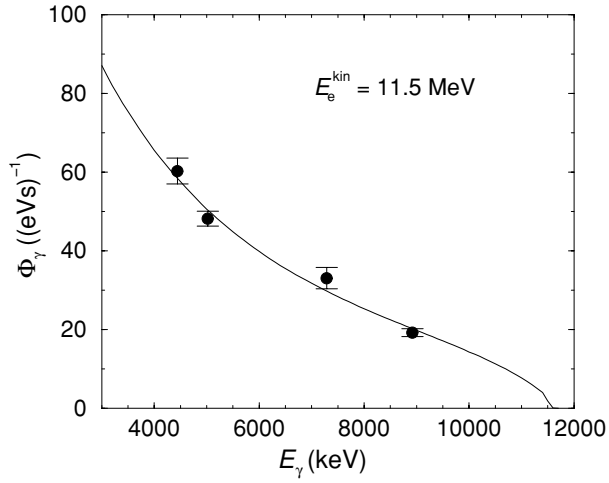

FIG. 2. Absolute photon flux at the target deduced from intensities of four known transitions in ^{11}B (circles) using the detector efficiency calculated with GEANT4.

C. Determination of the photoabsorption cross section

To determine the dipole-strength distribution, the experimental spectrum has to be corrected for detector response, for absolute efficiency, and for absolute photon flux. Besides, background radiation and radiation caused by atomic processes induced by the impinging photons in the ^{139}La target have to be taken into account. In a first step, spectra of the room background adjusted to the intensities of the 1460.5 keV transition (decay of ^{40}K) and 2614.9 keV transition (decay of ^{208}Tl) in the in-beam spectrum were subtracted. To correct the in-beam spectrum for detector response, spectra of monoenergetic γ rays were calculated in steps of 10 keV by using the program package GEANT4 [24]. Starting from the high-energy end of the in-beam spectrum, the simulated spectra were subtracted sequentially. The reliability of the simulation was tested by comparing simulated spectra with measured ones, as described in Refs. [6,7].

The absolute efficiencies of the HPGe detectors were determined experimentally using ^{22}Na, ^{60}Co, ^{65}Zn, ^{138}Ba, ^{137}Cs, and ^{226}Ra calibration sources. For further analysis, an efficiency curve calculated with GEANT4 and scaled to the absolute experimental values was used. Recent measurements of the detector efficiency using various (p,γ) reactions at the FZD Tandetron accelerator have proven that the GEANT4 simulations reproduce the experimental efficiencies within their uncertainties up to about 9 MeV [25]. The absolute photon flux was determined using the known integrated scattering cross sections of levels in ^{11}B. For interpolation, the photon flux was calculated using a code [26] based on the approximation given in Ref. [27] and including a screening correction according to Ref. [28]. This flux was corrected for absorption in the Al absorber placed behind the radiator and was then adjusted to the experimental values, as shown in Fig. 2.

To deduce the correct dipole-strength distribution, inelastic transitions have to be sorted out and the ground-state transitions have to be corrected for their branching ratios b_0. We have used statistical methods to estimate the intensities of branching transitions to low-lying excited levels and the branching ratios of the ground-state transitions. This method has also been applied in our earlier photon-scattering experiments at ELBE [6–10].

By using simulations, we corrected the spectrum, including events of the two detectors at 127°. At first, a spectrum of the ambient background adjusted to the intensities of the transitions from the decay of ^{40}K and ^{208}Tl in the in-beam spectrum was subtracted. To correct the spectrum for the detector response, spectra of monoenergetic γ rays were calculated in steps of 10 keV using the simulation code GEANT4. Starting from the high-energy end of the experimental spectrum, the simulated spectra were subtracted sequentially. After this correction, the peaks of the transitions in ^{11}B were subtracted. The background produced by atomic processes in the ^{139}La target was obtained from a GEANT4 simulation using the absolute photon flux deduced from the intensities of the transitions in ^{11}B (cf. Fig. 2). The corresponding background spectrum multiplied with the efficiency curve and with the measuring time is also displayed in Fig. 1.

As can be seen in Fig. 1, the continuum in the spectrum of photons scattered from ^{139}La is clearly higher than the background caused by atomic scattering processes. This continuum may be formed by a large number of nonresolvable transitions with small intensities, which are a consequence of the increasing nuclear level density at high energy and of Porter-Thomas fluctuations of the partial widths [29] in connection with the finite detector resolution. The relevant intensity of the photons resonantly scattered from ^{139}La is obtained from a subtraction of the atomic background from the response-corrected experimental spectrum. The remaining intensity distribution includes the intensity contained in the resolved peaks as well as the intensity of the "nuclear" continuum. The scattering cross sections $\sigma_{\gamma\gamma'}$ derived from this intensity distribution for energy bins of 100 keV are shown in Fig. 3. These values are compared with those deduced from the resolved transitions given in Table I. The two curves have similar structures caused by the prominent peaks. However,

TABLE I. Levels above 5 MeV assigned to ^{139}La.

E_x(keV)[a]	I_s(eVb)[b]	$g\Gamma_0^2/\Gamma$(meV)[c]
5380.6(6)	20(6)	151(47)
5389.8(12)	13(8)	95(58)
5406.8(13)	16(11)	120(86)
5423.1(7)	25(8)	192(63)
5545.4(7)	7(3)	55(25)
5552.7(9)	5(3)	40(26)
5572.0(11)	19(10)	153(79)
5582.1(10)	17(8)	138(61)
5594.8(7)	25(7)	206(57)
5620.4(8)	13(5)	110(40)
5658.8(7)	19(5)	158(41)
5688.1(5)	10(4)	88(30)
5708.6(7)	24(11)	207(89)
5716.5(6)	35(15)	296(126)
5723.0(3)	48(24)	409(209)
5811.3(8)	15(10)	131(90)
5830.9(9)	10(5)	90(41)
5848.9(6)	15(5)	133(41)
5940.2(8)	29(9)	264(79)
5984(2)	7(4)	62(37)
6015.5(8)	19(5)	181(45)
6047.1(14)	11(4)	101(41)
6077.9(11)	33(9)	314(89)
6097.8(12)	34(8)	326(76)
6112.0(15)	26(7)	257(67)
6131.1(9)	37(8)	361(78)
6150.8(10)	34(8)	331(82)
6178(3)	13(5)	125(47)
6194.1(9)	46(8)	456(82)
6214.2(5)	82(10)	828(105)
6233.2(8)	48(8)	486(84)
6249(2)	23(7)	232(71)
6260(2)	27(8)	271(79)
6269.5(12)	58(11)	595(109)
6301.1(6)	41(6)	424(65)
6326.1(6)	47(7)	495(72)
6354.8(5)	76(10)	795(101)
6366.5(10)	35(7)	365(72)
6383.5(5)	54(14)	568(143)
6402.6(9)	81(33)	869(347)
6435(2)	19(8)	201(82)
6441.9(11)	53(11)	567(115)
6450.9(4)	89(12)	961(131)
6465.3(7)	33(7)	354(81)
6483.8(16)	35(20)	381(213)
6491.3(8)	52(22)	574(245)
6501.4(6)	49(18)	542(201)
6526.7(6)	33(5)	370(61)
6539.6(5)	49(7)	542(73)
6549.6(8)	28(5)	315(59)
6619.4(6)	12(4)	132(46)
6651.3(7)	52(12)	594(142)
6674.8(8)	26(9)	303(108)
6713.0(6)	44(8)	516(93)
6723.8(15)	15(5)	182(60)
6755.8(7)	65(15)	769(173)
6767.6(18)	28(8)	328(101)
6875.4(8)	59(23)	729(286)
6889.9(8)	59(17)	732(211)
6901.1(10)	45(13)	563(161)
6926.3(8)	72(40)	895(495)
6969.0(6)	28(7)	355(95)
6983.4(7)	23(6)	292(71)
7019.7(10)	15(4)	188(58)
7036.1(9)	17(4)	216(55)
7052.4(7)	21(5)	270(63)
7154.0(11)	10(3)	136(39)
7158(3)	8(3)	103(35)
7272.8(15)	8(7)	116(90)
7320.0(8)	14(5)	191(68)
7327.2(8)	14(4)	194(61)
7370.0(8)	18(4)	250(56)
7400.0(7)	22(4)	315(62)
7414.0(7)	24(5)	338(70)
7444.9(12)	18(6)	267(85)
7451.1(9)	25(7)	357(98)
7462.8(7)	23(6)	337(89)
7472.0(9)	20(7)	293(97)
7506.7(7)	30(6)	442(89)
7552.7(8)	16(6)	240(94)
7562.1(4)	15(5)	224(78)
7570.2(11)	12(4)	173(60)
7579.8(6)	21(5)	313(73)
7591.6(11)	12(4)	176(54)
7599.1(7)	18(4)	264(61)
7636.2(5)	9(3)	131(41)
7661.3(18)	8(5)	128(83)
7667(3)	25(5)	376(75)
7678.6(16)	16(2)	238(38)
7684.7(9)	27(3)	416(45)
7692.4(12)	21(2)	325(38)
7699(3)	9(2)	134(32)
7765.1(13)	6(5)	100(71)
7789.4(13)	6(4)	95(62)
7905.2(6)	23(6)	374(94)
7912.5(7)	23(3)	367(41)
7922.2(9)	17(5)	277(85)
7961(3)	5(3)	78(51)
7972.3(7)	21(5)	351(78)
8551.5(6)	7(3)	127(53)
8595.7(5)	10(2)	186(46)

[a]Excitation energy. The uncertainty in parentheses is given in units of the last digit. This value was deduced from the γ-ray energy measured at 127° by including a recoil and Dopppler-shift correction.

[b]Energy-integrated scattering cross section deduced from intensities measured at 127°.

[c]Partial width of the ground-state transition Γ_0 multiplied with the branching ratio Γ_0/Γ and the statistical factor $g = (2J+1)/(2J_0+1)$.

the curve including also the continuum part of the spectrum contains altogether a strength that is by a factor of about 5 greater than the strength of the resolved peaks only.

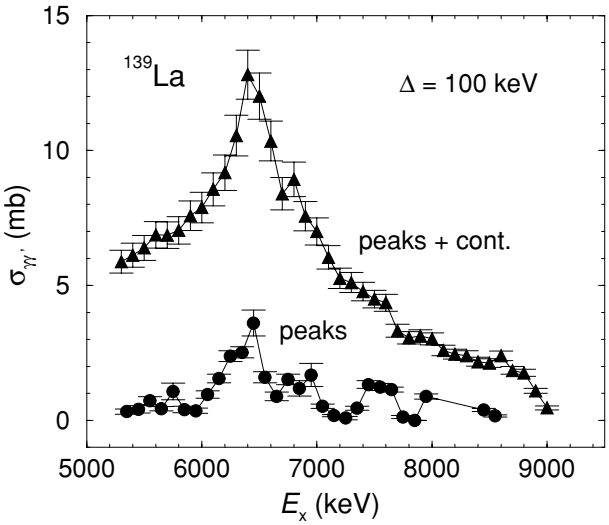

FIG. 3. Scattering cross sections in ^{139}La, derived as $\sigma_{\gamma\gamma'} = \sum_\Delta I_s/\Delta$, not corrected for branching and averaged over energy bins of $\Delta = 100$ keV, as derived from the difference of the experimental spectrum and the atomic background shown in Fig. 1 ("peaks + cont.," triangles) and from the resolved peaks only ("peaks," circles).

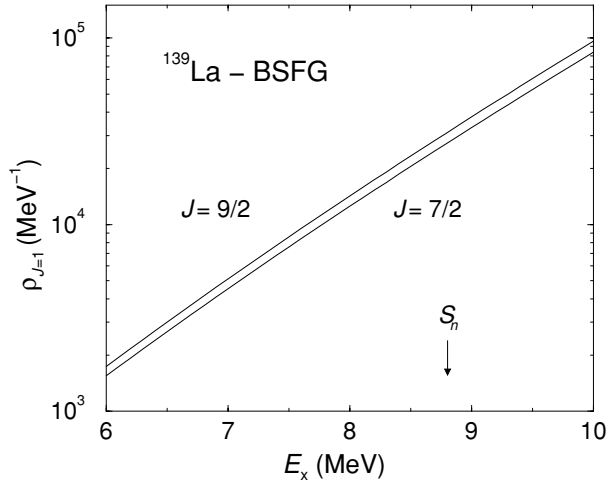

FIG. 4. Level density for $J = 7/2$ and $J = 9/2$ states in ^{139}La, including both parities as a function of the excitation energy, calculated according to the BSFG model with the parameters given in Ref. [33].

The full intensity distribution (resolved peaks and continuum) contains ground-state transitions and, in addition, branching transitions to lower lying excited states (inelastic transitions) as well as transitions from those states to the ground state (cascade transitions). The different types of transitions cannot be unambiguously distinguished. However, for the determination of the photoabsorption cross section and the partial widths Γ_0, the intensities of the ground-state transitions are needed. Therefore contributions of inelastic and cascade transitions have to be subtracted from the spectra. We corrected the intensity distributions by simulating γ-ray cascades [30] from the levels in the whole energy range analogously to the strategy of the Monte Carlo code DICEBOX [31]. In these simulations, 1000 level schemes (nuclear realizations) starting from the $7/2^+$ ground state and including states with $J = 3/2, 5/2, 7/2, 9/2$, and $11/2$ were created. We apply the statistical methods also for the low-energy part of the level scheme instead of using experimentally known low-lying levels in ^{139}La because this would require the knowledge of the partial decay widths of all transitions populating these fixed levels. Fluctuations of the nearest-neighbor spacings were taken into account according to the Wigner distribution (see, e.g., Ref. [32]). The partial widths of the transitions to low-lying levels were assigned using a priori known strength functions for $E1$, $M1$, and $E2$ transitions. Fluctuations of the partial widths were treated by applying the Porter-Thomas distribution [29].

Level densities were calculated using the back-shifted Fermi-gas (BSFG) model with the parameters $a = 13.02(32)\,\mathrm{MeV}^{-1}$ and $E_1 = -0.45(5)$ MeV adjusted to experimental level densities [33]. In the individual nuclear realizations, the values of a and E_1 were varied within their uncertainties. The resulting mean values of the level densities of all nuclear realizations for $J = 7/2$ and $J = 9/2$ states in ^{139}La are plotted in Fig. 4. We assumed equal level densities for states with positive and negative parities of the same spin. This assumption has recently been justified by the good agreement of level densities predicted by the BSFG model with experimental level densities of 1^+ states in the energy range from 5 to 10 MeV obtained from the ^{90}Zr(^{3}He,t)^{90}Nb reaction [34] and with experimental level densities of 2^+ and 2^- states in ^{90}Zr studied in the ^{90}Zr(e, e') and ^{90}Zr(p, p') reactions [35].

For the $E1$, $M1$, and $E2$ photon strength functions, we used Lorentzian parametrizations [36]. The parameters of the Lorentzian for the $E1$ strength were determined from a fit to (γ,n) data taken from Ref. [37] and scaled with a factor of 0.85 following the suggestion in Ref. [38]. The obtained parameters are energy of the maximum $E_0 = 15.24$ MeV, width $\Gamma = 4.47$ MeV, and cross section at the maximum $\sigma_0 = 286$ mb. Note that these values of σ_0 and Γ are consistent with the Thomas-Reiche-Kuhn sum rule [39], resulting in $\pi/2\sigma_0\Gamma = 60NZ/A$ MeV mb. The parameters for the $M1$ and $E2$ strengths were taken from global parametrizations of $M1$ spin-flip resonances and $E2$ isoscalar resonances, respectively [40].

Spectra of γ-ray cascades were generated for groups of levels in 100 keV bins in each of the 1000 nuclear realizations. For illustration, the intensity distributions of transitions depopulating levels in a 100 keV bin around the highest used energy of 9 MeV as resulting from 10 individual nuclear realizations are shown in Fig. 5. Because, in the nuclear realizations, the levels were created randomly starting from the ground state instead of starting with the lowest excited states in the accessible spin range, lying at 166 and 1219 keV, the distribution of the branching transitions continues to the energy bin of the ground-state transitions.

These spectra resemble qualitatively the ones measured in an experiment on ^{90}Zr using monoenergetic photons [41]. Starting from the high-energy end of the experimental spectrum, which contains ground-state transitions only, the simulated intensities of the ground-state transitions were normalized to the experimental ones in the considered bin,

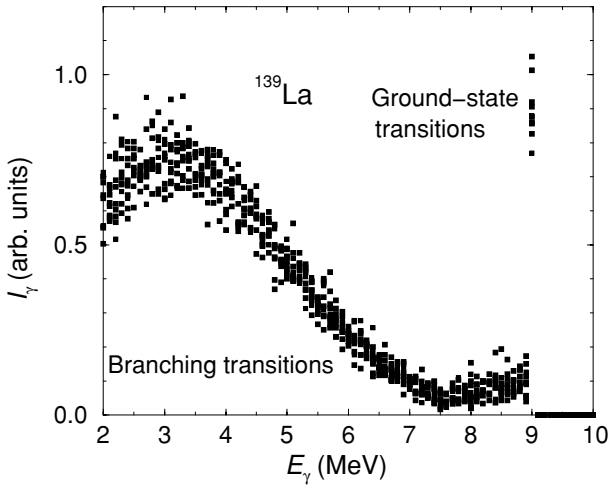

FIG. 5. Simulated intensity distributions depopulating levels in a 100 keV bin around 9 MeV. The squares depict the intensities obtained from 10 individual nuclear realizations.

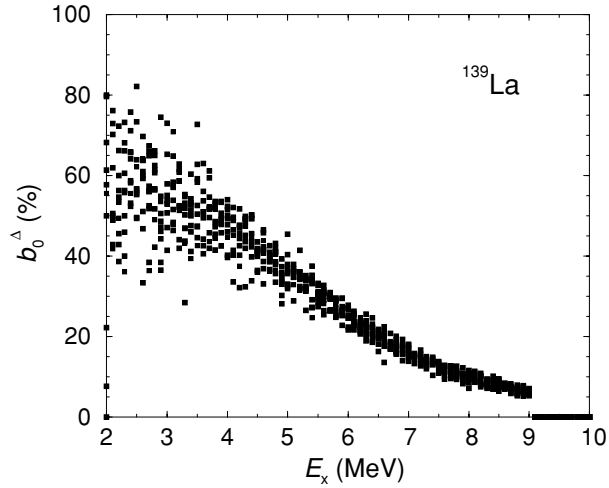

FIG. 6. Branching ratios of ground-state transitions as obtained from the simulations of γ-ray cascades for ^{139}La. The squares represent the values of 10 individual nuclear realizations.

and the intensity distribution of the branching transitions was subtracted from the experimental spectrum. Applying this procedure step by step for each energy bin, moving toward the low-energy end of the spectrum, we obtain the intensity distribution of the ground-state transitions. Simultaneously, the branching ratios b_0^Δ of the ground-state transitions are deduced for each energy bin Δ. In an individual nuclear realization, the branching ratio b_0^Δ is calculated as the ratio of the sum of the intensities of the ground-state transitions from all levels in Δ to the total intensity of all transitions depopulating those levels to any low-lying levels, including the ground state [6–10].

By dividing the summed intensities in a bin of the experimental intensity distribution of the ground-state transitions by the corresponding branching ratio, we obtain the absorption cross section for a bin as $\sigma_\gamma^\Delta = \sigma_{\gamma\gamma}^\Delta / b_0^\Delta$. Finally, the absorption cross sections of each bin were obtained by averaging over the values σ_γ^Δ of the 1000 nuclear realizations. For the uncertainty of the absorption cross section, a 1σ deviation from the mean has been taken.

To get an impression of the branching ratios, the individual values of 10 nuclear realizations are shown in Fig. 6. The mean branching ratio decreases from about 60% for states at 2 MeV to about 10% at the neutron-separation energy of 8.8 MeV.

The photoabsorption cross section for ^{139}La obtained from the present data and the analysis just described is shown in Fig. 7, together with cross sections deduced from (γ,n) experiments [19,37]. The (γ,p) cross section calculated with the code TALYS [42] is negligibly small and outside the range of Fig. 7. The total photoabsorption cross section has been deduced by combining the present (γ,γ') data and the (γ,n) data of Ref. [37]. In Fig. 8, this total cross section is compared with a Lorentz curve with the parameters given earlier. The extension of the GDR to energies below the particle threshold by a Lorentz curve was suggested in Ref. [43]. As can be seen in Fig. 8, the experimental cross section includes considerable enhanced strength with respect to the approximation of the GDR by a Lorentz curve in the energy range from about 6 to 10 MeV, which may indicate a PDR. Note that this enhanced strength shows two peaks at about 6.5 and 9 MeV, respectively. In the following, we will compare the dipole strength in ^{139}La with the results of calculations in the framework of a quasiparticle-random-phase approximation with instantaneous shape sampling (ISS-QRPA).

III. ISS-QRPA CALCULATIONS

The QRPA [39,44] is an appropriate method to describe the photoexcitation spectrum of both the vibrational states with individual levels below the neutron-separation energy and the hugely excited part of the continuous level structure at higher energies, known as the GDR. This approach was extensively used to interpret our measured low-energy dipole strength distributions in mass $A = 90 - 100$ nuclides with spherical as well as deformed equilibrium shapes [7,9,10,45]. In this

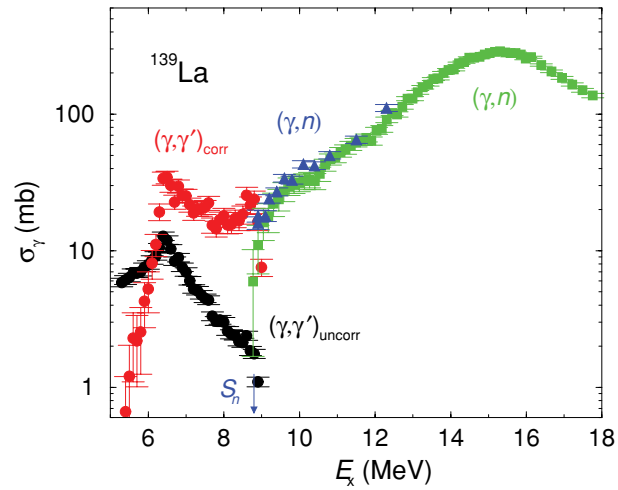

FIG. 7. (Color online) Uncorrected (black circles) and corrected (red circles) photoabsorption cross sections deduced from the present experiment in comparison with (γ,n) data from Ref. [19] (blue triangles) and Ref. [37] (green squares).

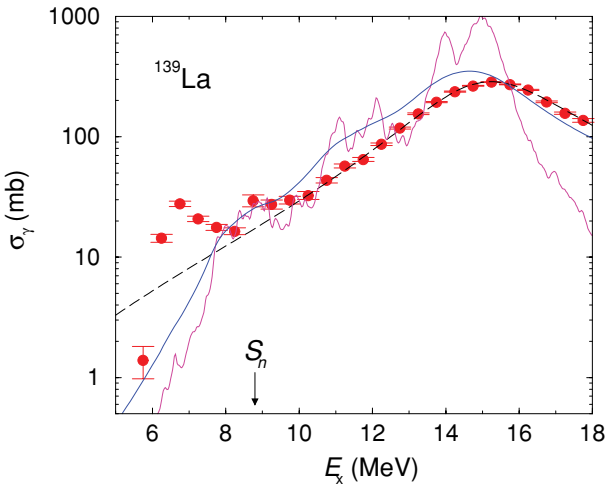

FIG. 8. (Color online) Total photoabsorption cross section of ^{139}La obtained by combining the present (γ,γ') data and the (γ,n) data of Ref. [37]. The data were averaged over 0.5 MeV bins to reduce statistical fluctuations. The black dashed line represents a Lorentz distribution with the parameters given in the text. The solid lines are results of the ISS-QRPA calculations discussed in Sec. III. The ISS-QRPA solutions were folded with Lorentzians of 0.1 MeV width (magenta line) and of an energy-dependent width according to $\Gamma = \alpha E^2$ MeV with $\alpha = 0.014$ MeV^{-1} (blue line).

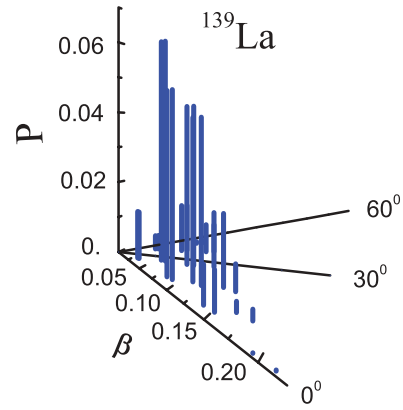

FIG. 9. (Color online) Probability distribution of instantaneous shapes in the β-γ plane.

work, we apply a recent extension of the standard QRPA called ISS, which accounts for possible shape fluctuations in the ground state that may change the dipole strength distributions. As described in Ref. [20], a series of QRPA calculations is performed that sample instantaneous quadrupole shapes of the collective motion in the nuclear ground state. The total absorption cross section is found by superimposing all these samples according to their probabilities, which are calculated using the interacting-boson approximation (IBA). The parameters of the IBA were derived from the ratios $E(4_1^+)/E(2_1^+)$, $E(2_2^+)/E(2_1^+)$, and $E(0_2^+)/E(2_1^+)$ in the even-even neighbors ^{138}Ba and ^{140}Ce, and the boson charge was deduced from the $B(E2, 2_1^+ \rightarrow 0_1^+)$ values in those nuclides. Like the usual QRPA approach, the ISS-QRPA is based on a Hamiltonian composed of a mean-field Hamiltonian $h_{\rm MF}$ and a residual interaction $V_{\rm res}$ given by the following expression:

$$H_{E1}^{\rm QRPA} = h_{\rm MF} - \frac{1}{2}\sum_{t=0,1}\sum_{\mu=-1,+1}\kappa^t_{1\mu}\,Q^t_{1\mu}\,Q^t_{1-\mu} - \frac{1}{2}\sum_{t=0,1}\sum_{\mu=-3,+3}\kappa^t_{3\mu}\,Q^t_{3\mu}\,Q^t_{3-\mu}. \quad (3)$$

The term $h_{\rm MF}$ is a quasiparticle Hamiltonian that consists of a Woods-Saxon mean field and a monopole pairing potential [46]. In this part, the instantaneous shape of the sample is defined by a deformed Woods-Saxon potential implying the shape parameters β and γ. The residual interaction $V_{\rm res}$ in the Hamiltonian in Eq. (3) comprises isoscalar ($t = 0$) and isovector ($t = 1$) parts of the dipole-dipole ($\lambda = 1$) and octupole-octupole ($\lambda = 3$) interaction, where the multipole operators are defined as $Q^t_{\lambda\mu} = [r^\lambda Y_{\lambda\mu}]^\pi + (-1)^t[r^\lambda Y_{\lambda\mu}]^\nu$. The constants $\kappa^{t=1}_{\lambda\mu}$ of the repulsive isovector interaction are adjusted such that they reproduce the energy of the maximum of the GDR in accordance with the experimental value. To remove the effects of the spurious center-of-mass motion, the suppression method described in Ref. [47] has been applied. This method allows us also to calculate the transition strengths without assuming any effective charge for the neutrons and using directly the bare proton charge e_π in the transition operator, that is,

$$\hat{M}(E1)_\mu = e_\pi \sum_{i=1}^{Z}[rY_{1\mu}]_i. \quad (4)$$

Instantaneous shapes obtained for ^{139}La are shown in Fig. 9. These shapes are distributed over a range of the quadrupole deformation from about $\beta = 0.05$ to about $\beta = 0.20$, with a maximum around $\beta = 0.07$, while the triaxial deformation is rather indefinite, taking values between about $\gamma = 0^\circ$ and $\gamma = 60^\circ$. This probability distribution corresponds to a soft spherical nucleus that carries out large shape fluctuations.

The $E1$ photoabsorption cross sections for ^{139}La calculated in ISS-QRPA are shown in Fig. 8. For comparison with the experimental values, the cross sections of the calculated ISS-QRPA states were folded with Lorentzians. Using a fixed width of 0.1 MeV for the Lorentzians, the calculated curve has substantial fluctuations, and its maximum is much too high and too narrow compared with the experimental GDR peak region around 15.2 MeV. Taking into account collisional damping by applying a Lorentzian with an energy-dependent width $\Gamma = \alpha E^2$ MeV, with $\alpha = 0.014$ MeV^{-1}, as suggested in Ref. [20], the calculated curve gets more smooth. Moreover, the calculated curve has two maxima at about 9 MeV and 11.5 MeV, respectively, which are relicts of the underlying particle-hole spectrum. These two maxima may have the same origin as the experimental ones observed at about 6.5 and 9 MeV, respectively, but do not reproduce the right energies.

IV. CONCLUSION

The dipole-strength distribution in ^{139}La up to the neutron-separation energy has been studied in photon-scattering experiments at the ELBE accelerator using an electron kinetic

energy of 11.5 MeV. The intensity distribution obtained from the measured spectra after a correction for detector response and a subtraction of atomic background in the target contains a quasicontinuum in addition to resolved peaks. To obtain information about the intensities of inelastic transitions to low-lying levels, we have applied statistical methods. By means of simulations of γ-ray cascades, intensities of branching transitions could be estimated and subtracted from the experimental intensity distribution, and the intensities of the remaining ground-state transitions could be corrected on average for their branching ratios. The photoabsorption cross section obtained in this way from the present (γ,γ') experiment connects continuously to (γ,n) data and gives new information about the extension of the dipole-strength distribution toward energies around and below the threshold of the (γ,n) reaction. In comparison with a straightforward approximation of the GDR by a Lorentz curve, we observe enhanced $E1$ strength in the energy range from 6 to 10 MeV, with two peaks at about 6.5 and 9 MeV, respectively. ISS-QRPA calculations predict also two resonance-like structures in the $E1$ strength, however, at a too-high energy of about 9 and 11.5 MeV, respectively.

ACKNOWLEDGMENTS

We thank the staff of the ELBE accelerator for cooperation during the experiments and A. Hartmann for technical assistance. We thank H. Utsunomiya for his teaching in the early stage of this work and in the photoneutron experiment. A.M. was supported by Forschungszentrum Dresden-Rossendorf and the Japanese Private School Promotion Foundation. F.D. and S.F. were supported by the German DFG (Grant No. KA2519/1-1) and by the US Department of Energy (Grant No. DE-FG02-95ER4093).

[1] M. Arnould and S. Goriely, Phys. Rep. **384**, 1 (2003).
[2] G. A. Bartholomew, E. D. Earle, A. J. Ferguson, J. W. Knowles, and M. A. Lone, Adv. Nucl. Phys. **7**, 229 (1973).
[3] A. Zilges, S. Volz, M. Babilon, T. Hartmann, P. Mohr, and K. Vogt, Phys. Lett. B **542**, 43 (2002).
[4] S. Volz, N. Tsoneva, M. Babilon, M. Elvers, J. Hasper, R.-D. Herzberg, H. Lenske, K. Lindenberg, D. Savran, and A. Zilges, Nucl. Phys. A **779**, 1 (2006).
[5] P. Adrich *et al.*, Phys. Rev. Lett. **95**, 132501 (2005).
[6] R. Schwengner *et al.*, Phys. Rev. C **76**, 034321 (2007).
[7] G. Rusev *et al.*, Phys. Rev. C **77**, 064321 (2008).
[8] R. Schwengner *et al.*, Phys. Rev. C **78**, 064314 (2008).
[9] N. Benouaret *et al.*, Phys. Rev. C **79**, 014303 (2009).
[10] G. Rusev *et al.*, Phys. Rev. C **79**, 061302(R) (2009).
[11] S. Goriely, Phys. Lett. B **436**, 10 (1998).
[12] S. Goriely, J. José, M. Hernanz, M. Rayet, and M. Arnould, Astron. Astrophys. **383**, L27 (2002).
[13] S. Goriely, M. Arnould, I. Borzov, and M. Rayet, Astron. Astrophys. **375**, L35 (2001).
[14] J. Audouze, Astron. Astrophys. **8**, 436 (1970).
[15] S. E. Woosley, D. H. Hartmann, R. D. Hoffman, and W. C. Haxton, Astrophys. J. **356**, 272 (1990).
[16] M. Scheck *et al.*, Phys. Rev. C **75**, 044313 (2007).
[17] N. Ryezayeva, T. Hartmann, Y. Kalmykov, H. Lenske, P. von Neumann-Cosel, V. Y. Ponomarev, A. Richter, A. Shevchenko, S. Volz, and J. Wambach, Phys. Rev. Lett. **89**, 272502 (2002).
[18] R. Schwengner *et al.*, Phys. Rev. C **81**, 054315 (2010).
[19] H. Utsunomiya *et al.*, Phys. Rev. C **74**, 025806 (2006).
[20] S. Q. Zhang, I. Bentley, S. Brant, F. Dönau, S. Frauendorf, B. Kämpfer, R. Schwengner, and A. Wagner, Phys. Rev. C **80**, 021307(R) (2009).
[21] R. Schwengner *et al.*, Nucl. Instrum. Methods A **555**, 211 (2005).
[22] F. Ajzenberg-Selove, Nucl. Phys. A **506**, 1 (1990).
[23] G. Rusev, A. P. Tonchev, R. Schwengner, C. Sun, W. Tornow, and Y. K. Wu, Phys. Rev. C **79**, 047601 (2009).
[24] S. Agostinelli *et al.*, Nucl. Instrum. Methods A **506**, 250 (2003).
[25] E. Trompler, diploma thesis, Technische Universität Dresden, 2009.
[26] E. Haug, Radiat. Phys. Chem. **77**, 207 (2008).
[27] G. Roche, C. Ducos, and J. Proriol, Phys. Rev. A **5**, 2403 (1972).
[28] F. Salvat, J. D. Martinez, R. Mayol, and J. Parellada, Phys. Rev. A **36**, 467 (1987).
[29] C. E. Porter and R. G. Thomas, Phys. Rev. **104**, 483 (1956).
[30] G. Rusev, Ph.D. thesis, Technische Universität Dresden, 2007.
[31] F. Bečvář, Nucl. Instrum. Methods A **417**, 434 (1998).
[32] T. A. Brody, J. Flores, J. B. French, P. A. Mello, A. Pandey, and S. S. M. Wong, Rev. Mod. Phys. **53**, 385 (1981).
[33] T. von Egidy and D. Bucurescu, Phys. Rev. C **80**, 054310 (2009).
[34] Y. Kalmykov *et al.*, Phys. Rev. Lett. **96**, 012502 (2006).
[35] Y. Kalmykov, C. Özen, K. Langanke, G. Martínez-Pinedo, P. von Neumann-Cosel, and A. Richter, Phys. Rev. Lett. **99**, 202502 (2007).
[36] P. Axel, Phys. Rev. **126**, 671 (1962).
[37] H. Beil, R. Bergere, P. Carlos, A. Lepretre, and A. Veyssiere, Nucl. Phys. A **172**, 426 (1971).
[38] B. L. Berman, R. E. Pywell, S. S. Dietrich, M. N. Thompson, K. G. McNeill, and J. W. Jury, Phys. Rev. C **36**, 1286 (1987).
[39] P. Ring and P. Schuck, in *The Nuclear Many Body Problem* (Springer, New York, 1980).
[40] T. Belgya *et al.*, IAEA Report No. RIPL-2, IAEA-TECDOC-1506, 2006, [http://www-nds.iaea.org/RIPL-2/].
[41] R. Alarcon, R. M. Laszewski, A. M. Nathan, and S. D. Hoblit, Phys. Rev. C **36**, 954 (1987).
[42] A. J. Koning, S. Hilaire, and M. C. Duijvestijn, AIP Conf. Proc. **769**, 1154 (2005).
[43] C. B. Dover, R. H. Lemmer, and F. J. W. Hahne, Ann. Phys. **70**, 458 (1972).
[44] D. J. Rowe, in *Nuclear Collective Motion* (Methuen, London, 1970).
[45] G. Rusev *et al.*, Phys. Rev. C **73**, 044308 (2006).
[46] F. Dönau, G. Rusev, R. Schwengner, A. R. Junghans, K. D. Schilling, and A. Wagner, Phys. Rev. C **76**, 014317 (2007).
[47] F. Dönau, Phys. Rev. Lett. **94**, 092503 (2005).